

## Ionization channel of continuum lowering in plasmas: effects of plasma screening, electric and magnetic fields

This content has been downloaded from IOPscience. Please scroll down to see the full text.

2013 J. Phys. B: At. Mol. Opt. Phys. 46 245701

(<http://iopscience.iop.org/0953-4075/46/24/245701>)

View [the table of contents for this issue](#), or go to the [journal homepage](#) for more

### Download details:

IP Address: 132.248.28.70

This content was downloaded on 11/11/2016 at 02:06

Please note that [terms and conditions apply](#).

You may also be interested in:

[Classical description of charge exchange involving He-like or Li-like ions in rydberg states in plasmas](#)

N Kryukov and E Oks

[STABLE CONIC-HELICAL ORBITS OF PLANETS AROUND BINARY STARS: ANALYTICAL RESULTS](#)

E. Oks

[Crossings of energy levels](#)

E Oks

[Semiclassical ionization dynamics of the hydrogen molecular ion](#)

T Bartsch and T Uzer

[B-splines in atomic and molecular physics](#)

H Bachau, E Cormier, P Decleva et al.

[Influence of Debye plasma on the cross section and linear polarization of x-ray radiation following inner-shell electron-impact excitation of highly charged Be-like Sc<sup>17+</sup> ions](#)

Zhan-Bin Chen, Chen-Zhong Dong, Jun Jiang et al.

# Ionization channel of continuum lowering in plasmas: effects of plasma screening, electric and magnetic fields

N Kryukov and E Oks

Physics Department, 206 Allison Lab, Auburn University, Auburn, AL 36849, USA

E-mail: [goks@physics.auburn.edu](mailto:goks@physics.auburn.edu)

Received 30 August 2013, in final form 23 October 2013

Published 27 November 2013

Online at [stacks.iop.org/JPhysB/46/245701](http://stacks.iop.org/JPhysB/46/245701)

## Abstract

Calculations of continuum lowering (CL) in plasmas evolved from ion sphere models to dicentre models of the plasma state. One of such theories—a percolation theory—calculated CL defined as an absolute value of energy at which an electron becomes bound to a macroscopic portion of plasma ions (a quasi-ionization). Previously one of us derived analytically the value of CL in the ionization channel which was disregarded in the percolation theory. In the present paper we study how the value of CL in the ionization channel is affected by plasma screening, electric and magnetic fields. We show that the screening and the magnetic field decrease the value of CL, inhibiting the ionization, while the electric field increases the value of CL, promoting the ionization. These results should be important for inertial fusion, x-ray lasers, powerful Z-pinchs, astrophysics and other applications of high-density plasmas. We also show that the screening stabilizes the nuclear motion of the corresponding Rydberg quasimolecules in some cases and destabilizes it in other cases.

(Some figures may appear in colour only in the online journal)

## 1. Introduction

Continuum lowering (hereafter, CL) is a fundamental concept of atomic physics in plasmas. It refers to the fact that the energy required to ionize is reduced compared to its value in vacuum. This is because highly excited states above a certain threshold disappear from the discrete spectrum. The higher the plasma density, the more significant CL becomes. It defines the existing energy states and affects their absorption and emission properties. CL is important for inertial fusion, x-ray lasers, astrophysics and other applications of high-density plasmas. It is usually included in most comprehensive simulations of atomic physics in plasmas. CL plays a key role in calculations of the equation of state, partition function, bound-free opacities and other collisional atomic transitions in plasmas.

CL has been studied for over 50 years—see, e.g., books/reviews [1–5] and references therein. Calculations of CL evolved from ion sphere models to dicentre models of the plasma state [3, 6–11]. One of such theories—a percolation theory [3, 8]—calculated CL defined as an absolute value of energy at which an electron becomes bound to a macroscopic

portion of plasma ions (a quasi-ionization). In 2001 one of us derived analytically the value of CL in the true-ionization channel which was disregarded in the percolation theory: a quasimolecule, consisting of the two ion centres plus an electron, can get ionized in the true sense of this word before the electron would be shared by more than two ions [12]. In other words, the distinction between the quasi-ionization (i.e., the percolation theory) and the true ionization is the following. The basic process in the percolation theory is the tunnelling of the electron between the two adjacent ionic potential wells. But this means that the electron is still a part of the quasimolecule consisting of the two adjacent ions and the electron, i.e., the electron is still bound. However, it is well-known from molecular physics that any molecule or quasimolecule can actually lose an electron, i.e., get truly ionized. This represents the true-ionization channel of CL—in addition to the quasi-ionization channel of the percolation theory.

It was also shown in [12] that, whether the electron is bound primarily by the smaller or by the larger out of two positive charges  $Z$  and  $Z'$ , makes a dramatic qualitative and quantitative difference for this ionization channel. The results

in [12] were obtained for circular states of the corresponding Rydberg quasimolecules.

Circular Rydberg states of atomic and molecular systems having one electron, in the quantal language correspond to  $|m| = n - 1 \gg 1$ , where  $m$  and  $n$  are the principal and magnetic electronic quantum numbers, respectively. They have been extensively studied both theoretically and experimentally [13–16]. Classically these states correspond to the electron orbit being a circle perpendicular to and centred at the internuclear axis.

In the present paper we study how three different factors affect the value of CL in the ionization channel. The first factor is the screening by plasma electrons that was disregarded in [12]. The second factor is an electric field. It represents (in a model way) a quasistatic ion microfield due to contributions of all ions except the two ions included in the dicentre. The third factor is a magnetic field. Relevant applications of the latter include (but are not limited to) laser fusion, where a strong magnetic field can be generated in the process of the laser–plasma interaction [17, 18], and powerful Z-pinchs used for producing x-ray and neutron radiation, ultra-high pulsed magnetic fields and for x-ray lasing (see, e.g., [19]). We show that the screening and the magnetic field decrease the value of CL, inhibiting the ionization, while the electric field increases the value of CL, promoting the ionization.

We also study the effect of the screening on crossings of energy terms and on the stability of the nuclear motion of the corresponding Rydberg quasimolecules. We show that the screening stabilizes the nuclear motion in the case of  $Z = 1$  and destabilizes it in the case of  $Z > 1$ .

## 2. Calculation of the effect of plasma screening on classical energy terms of Rydberg quasimolecules in circular states

Plasma screening of a test charge is a well-known phenomenon. For a hydrogen atom or a hydrogen-like ion (an H-atom, for short), it is effected by replacing the pure Coulomb potential by a screened Coulomb potential which contains a physical parameter—the screening length  $a$ . For example, the Debye–Hückel (or Debye) interaction of an electron with the electronic shielded field of an ion of charge  $Z$  is  $U(R) = -(Ze^2/R)\exp(-R/a)$ , where  $a = (kT/(4\pi e^2 N_e))^{1/2} \approx 1.304 \times 10^4 (10^{10}/N_e)^{1/2} T^{1/2} a_0$ , where  $N_e$  ( $\text{cm}^{-3}$ ) and  $T$  (K) are the electron density and temperature, respectively.

We study a two-Coulomb centre (TCC) system with the charge  $Z$  placed at the origin, and the  $Oz$  axis directed at the charge  $Z'$ , which is at  $z = R$ , the system being in a plasma of a screening length  $a$ . We consider the circular orbits of the electron which are perpendicular to the internuclear axis and centred on the axis.

Two quantities, the energy  $E$  and the projection  $L$  of the angular momentum on the internuclear axis are conserved in this configuration. We use cylindrical coordinates  $(\rho, \varphi, z)$ , which are related to the Cartesian coordinates as  $x = \rho \cos \varphi$ ,  $y = \rho \sin \varphi$ ,  $z = z$ , to write the equations for both:

$$E = \frac{1}{2}(\dot{\rho}^2 + \rho^2 \dot{\varphi}^2 + \dot{z}^2) - \frac{Z}{r} e^{-r/a} - \frac{Z'}{r'} e^{-r'/a} \quad (1)$$

$$L = \rho^2 \dot{\varphi}, \quad (2)$$

where  $r$  and  $r'$  are distances from the electron to  $Z$  and  $Z'$ . The circular motion implies that  $d\rho/dt = 0$ ; as the motion occurs in the plane perpendicular to the  $z$ -axis,  $dz/dt = 0$ . Further, expressing  $r$  and  $r'$  through  $\rho$  and  $z$ , and taking  $d\varphi/dt$  from (2), we have:

$$E = \frac{L^2}{2\rho^2} - \frac{Z}{\sqrt{\rho^2 + z^2}} e^{-\sqrt{\rho^2 + z^2}/a} - \frac{Z'}{\sqrt{\rho^2 + (R-z)^2}} e^{-\sqrt{\rho^2 + (R-z)^2}/a}. \quad (3)$$

With the scaled quantities

$$w = \frac{z}{R}, \quad p = \left(\frac{\rho}{R}\right)^2, \quad b = \frac{Z'}{Z}, \quad \varepsilon = -\frac{ER}{Z}, \\ \ell = \frac{L}{\sqrt{ZR}}, \quad \lambda = \frac{R}{a}, \quad r = \frac{ZR}{L^2} \quad (4)$$

our energy equation takes the form below:

$$\varepsilon = \frac{e^{-\lambda\sqrt{w^2+p}}}{\sqrt{w^2+p}} + \frac{b e^{-\lambda\sqrt{(1-w)^2+p}}}{\sqrt{(1-w)^2+p}} - \frac{\ell^2}{2p}. \quad (5)$$

We can seek the equilibrium points by finding partial derivatives of  $\varepsilon$  by the scaled coordinates  $w, p$  and setting them equal to zero. This will give the following two equations:

$$\frac{w e^{-\lambda\sqrt{w^2+p}}}{w^2+p} \left( \frac{1}{\sqrt{w^2+p}} + \lambda \right) = \frac{b(1-w) e^{-\lambda\sqrt{(1-w)^2+p}}}{(1-w)^2+p} \\ \times \left( \frac{1}{\sqrt{(1-w)^2+p}} + \lambda \right), \quad (6)$$

$$\frac{\ell^2}{p^2} = \frac{e^{-\lambda\sqrt{w^2+p}}}{w^2+p} \left( \frac{1}{\sqrt{w^2+p}} + \lambda \right) + \frac{b e^{-\lambda\sqrt{(1-w)^2+p}}}{(1-w)^2+p} \\ \times \left( \frac{1}{\sqrt{(1-w)^2+p}} + \lambda \right). \quad (7)$$

From the definitions of the scaled quantities (4), we have  $\ell^2 = 1/r$  and  $E = -(Z/R) \varepsilon$ . Since  $r = ZR/L^2$ , then  $E = -(Z/L)^2 \varepsilon/r$ , where  $r = 1/\ell^2$  can be obtained by solving (7) for  $\ell$ . Thus, the scaled energy without explicit dependence on  $R$  is  $\varepsilon/r$ , which we shall denote  $\varepsilon_1$ . Using this, equations (5)–(7) can be transformed into the following three master equations for this configuration:

$$\varepsilon_1 = \left( \frac{p(1 + \lambda\sqrt{w^2+p}) e^{-\lambda\sqrt{w^2+p}}}{(1-w)(w^2+p)^{3/2}} \right)^2 \\ \times \left( \frac{(1-w)(w^2+p)}{1 + \lambda\sqrt{w^2+p}} + \frac{w((1-w)^2+p)}{1 + \lambda\sqrt{(1-w)^2+p}} - \frac{p}{2} \right), \quad (8)$$

$$r = \frac{(1-w)(w^2+p)^{3/2} e^{\lambda\sqrt{w^2+p}}}{p^2(1 + \lambda\sqrt{w^2+p})}, \quad (9)$$

$$\frac{w(1 + \lambda\sqrt{w^2+p}) e^{-\lambda\sqrt{w^2+p}}}{(w^2+p)^{3/2}} \\ = \frac{b(1-w)(1 + \lambda\sqrt{(1-w)^2+p}) e^{-\lambda\sqrt{(1-w)^2+p}}}{((1-w)^2+p)^{3/2}}. \quad (10)$$

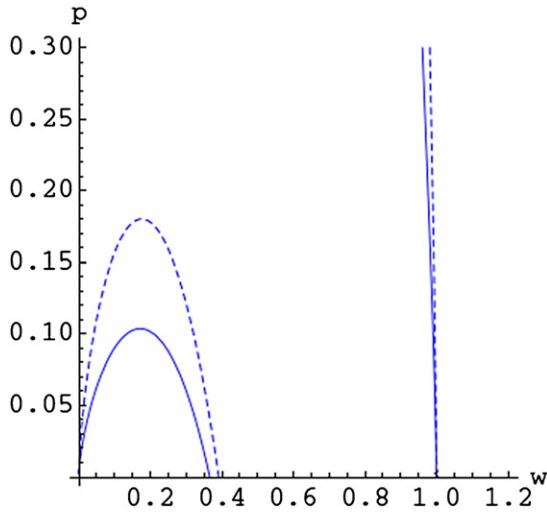


**Figure 1.** Contour plot of equation (10) for  $b = 3$ ,  $\lambda = 0.1$  (solid curves) and for  $b = 3$ ,  $\lambda = 2$  (dashed curves).

The quantities  $\varepsilon_1$  and  $r$  now depend only on the coordinates  $w$  and  $p$  (besides the constant  $\lambda$ ). Therefore, if we solve (10) for  $p$  and substitute it to (8) and (9), we obtain the parametric solution for the energy terms  $\varepsilon_1(r)$  with the parameter  $w$  for the given  $b$  and  $\lambda$ .

Equation (10) does not allow an exact analytical solution for  $p$ . Therefore, we will use an approximate analytical method.

Figure 1 is the contour plot of this equation for  $b = 3$  and  $\lambda = 0.1$  (solid curves) and  $\lambda = 2$  (dashed curves).

As in [21, 22], which presented the study of the same  $ZeZ'$  system for  $\lambda = 0$ , the plot has two branches, the left one spanning from  $w = 0$  to  $w = w_1$ , and the right one from the asymptote  $w = w_3$  to  $w = 1$ . Here  $w_1$  is a solution of the equation

$$(1 - w_1)^2(1 + \lambda w_1) e^{\lambda(1-2w_1)} = b w_1^2(1 + \lambda(1 - 2w_1)), \quad (11)$$

in the interval  $0 < w_1 < 1$ , and  $w_3$  does not depend on  $\lambda$  and equals  $b/(1 + b)$ —the same as in [21, 22] for  $\lambda = 0$ . As  $\lambda$  increases,  $w_1$  and the  $p$ -coordinate of the maximum of the left branch increase, but the general shape of both curves is preserved (figure 1).

An approximation was made for small values of  $\lambda$ . Approximating (10) in the first power of  $\lambda$ , we obtain the expression involving only the second and higher powers of  $\lambda$ . Therefore, an attempt was made using the value of  $p(w)$  for  $\lambda = 0$  presented in [22], which we shall denote as  $p_0$ ; it is the same as the squared quantity in equation (11) in [22]. Further, taking the higher powers of  $\lambda$  into account, we obtained the next-order approximation for  $p(w)$ :

$$p(w) = p_0 + \frac{\lambda^2}{6}(1 - 2w)(1 + (1 - 2w)) \times \left( \frac{w^{2/3} + b^{2/3}(1 - w)^{2/3}}{w^{2/3} - b^{2/3}(1 - w)^{2/3}} \right)^2 \quad (12)$$

where

$$p_0 = \frac{w^{2/3}(1 - w)^{4/3} - b^{2/3}w^2}{b^{2/3} - w^{2/3}(1 - w)^{-2/3}} \quad (13)$$

—the zero- $\lambda$  value as in equation (11) in [22].

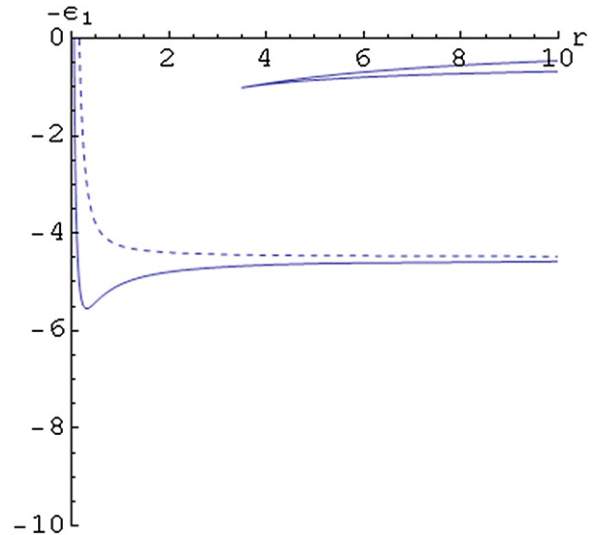


**Figure 2.** Approximate classical energy terms for  $b = 3$  at  $\lambda = 0.1$  (solid curves) and at  $\lambda = 0.3$  (dashed curve). For the top two terms (forming a V-crossing) the solid and dashed curves practically coincide.

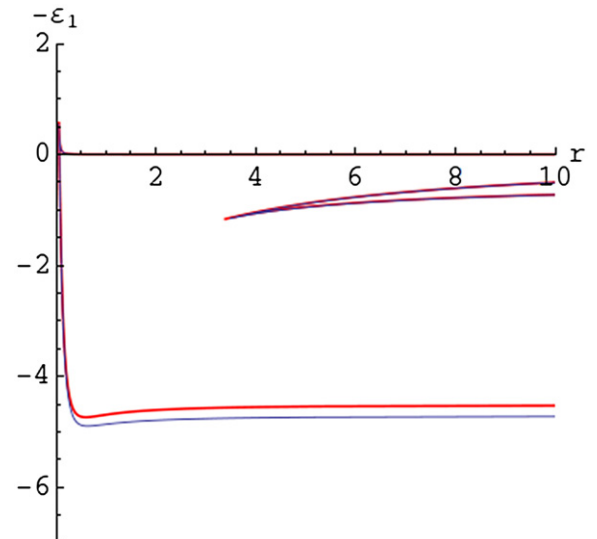


**Figure 3.** Numerical (red, thicker lines) and analytical (blue, thinner lines) classical energy terms for  $b = 3$  at  $\lambda = 0.2$ .

Equation (11) of the present paper can be approximated by substituting  $1 + \lambda(1 - 2w_1)$  in place of  $\exp(\lambda(1 - 2w_1))$ , which will render it a fourth-degree polynomial in  $w_1$ .

Substituting (12) into (8) and (9), we obtain the approximate parametric solution for the classical energy terms  $-\varepsilon_1(r)$  by running the parameter  $w$  on  $0 < w < w_1$  and  $w_3 < w < 1$ . Empirically, by comparison with the numerical results, it was found that using the value of  $p$  from (13) on the  $0 < w < w_1$  range and from (12) on the  $w_3 < w < 1$  range gives the best approximate results. Figure 2 shows the approximate classical energy terms for  $b = 3$  and different values of  $\lambda$ .

A numerical solution has also been made. We solved (10) numerically for  $p$  and substituted it into (8) and (9), thus obtaining the parametric dependence  $\varepsilon_1(r)$  via parameter  $w$  for the given  $b$  and  $\lambda$ . It confirmed that the analytical solution was a good approximation for  $\lambda < 0.3$ . Figure 3 depicts terms plotted for selected values of  $\lambda$ .

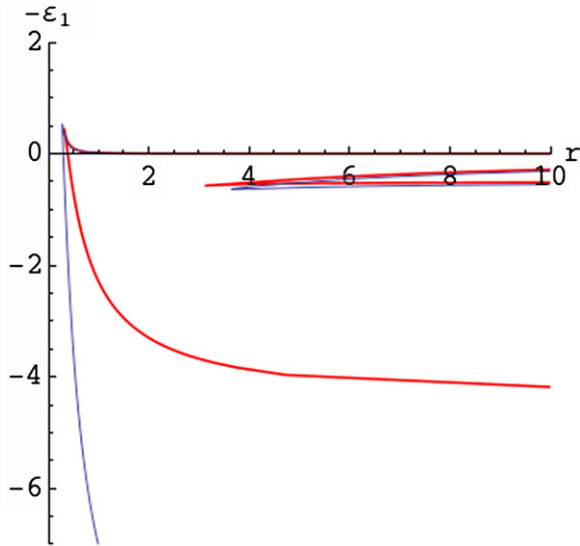


**Figure 4.** Numerical (red, thicker lines) and analytical (blue, thinner lines) classical energy terms for  $b = 3$  at  $\lambda = 1$ .

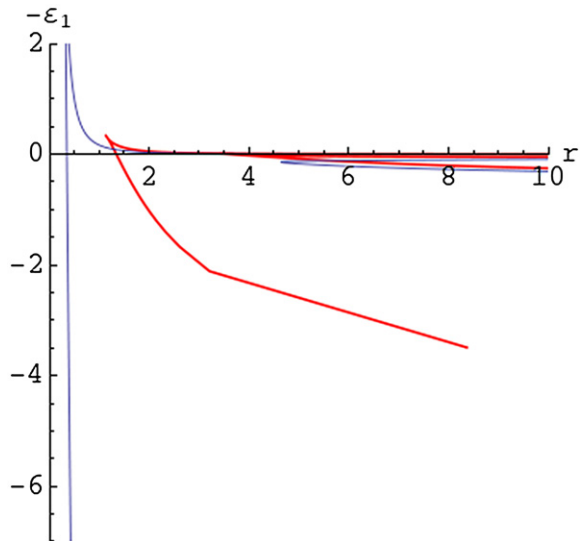


**Figure 5.** Numerical (red, thicker lines) and analytical (blue, thinner lines) classical energy terms for  $b = 3$  at  $\lambda = 3$ .

The following clarification should be made. The plots in figures 3–5 represent ‘classical energy terms’ of the same symmetry. (In the physics of diatomic molecules, the terminology ‘energy terms of the same symmetry’ means the energy terms of the same projection of the angular momentum on the internuclear axis.) For a given  $R$  and  $L$ , the classical energy  $E$  takes only several *discrete* values. However, as  $L$  varies over a *continuous* set of values, so does the classical energy  $E$  (as it should be in classical physics).

We note that in case of small or moderate  $\lambda$ , we observe four terms, both pairs of which have a V-type crossing—the common point of two terms which also corresponds to the minimum internuclear distance for both (the shape of the two terms next to the crossing resembles a rotated letter V). As an example, we shall take the plot of the terms for  $\lambda = 1$  (figure 4) and number the lowest term 1 and the highest term 2; the remaining terms will be numbered 3 and 4, from the

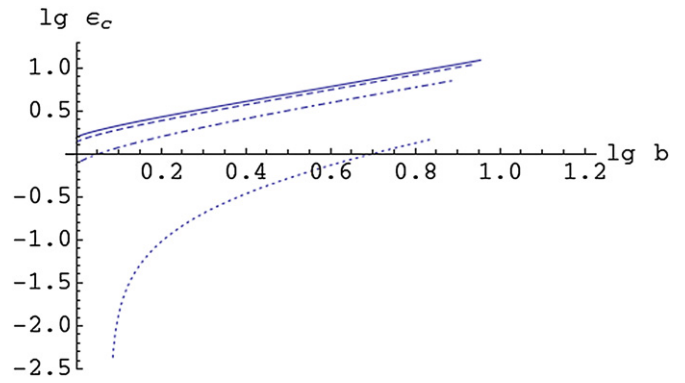


**Figure 6.** The plot of the continuum lowering (CL) energy versus  $b$  on a double-logarithmic scale for  $\lambda = 0$  (solid curve),  $\lambda = 0.1$  (dashed curve),  $\lambda = 0.5$  (dot–dashed curve) and  $\lambda = 2$  (dotted curve).

lower one to the higher one. Therefore, terms 1 and 2 and terms 3 and 4 undergo V-type crossings, to which we shall refer to as V12 and V34.

### 3. Plasma screening effects on the continuum lowering in the ionization channel

Our analysis of the stability of the electronic motion shows results similar to those obtained by one of us previously in [21, 22]. Namely, term 3 corresponds to a stable motion while term 4—to an unstable motion. So, *the crossing point of terms 3 and 4 corresponds to the transition from the stable motion to the unstable motion, leading the electron to the zero energy (i.e., to the free motion) along term 4, which constitutes the ionization of the molecule.*

Therefore, we arrive at the following. For the ionization of the hydrogen-like ion of the nuclear charge  $Z_{\min}$  perturbed by the charge  $Z_{\max}$ , it is sufficient to reach the scaled energy  $\varepsilon_c(b) = \varepsilon(w_{V34}(b), b) < 0$ . At that point, the electron switches to the unstable motion and the radius of its orbit increases without a limit. This constitutes CL by the amount of  $Z\langle 1/R \rangle |\varepsilon(w_{V34}(b), b)|$ , where  $\langle 1/R \rangle$  is the value of the inverse distance of the nearest neighbour ion from the radiating ion averaged over the ensemble of perturbing ions.

Thus, obtaining CL in the ionization channel requires calculations of the scaled energy  $\varepsilon$  at the crossing point  $w_{V34}$  of terms 3 and 4. These calculations are presented in appendix A.

CL for the ‘default’ ( $\lambda = 0$ ) TCC system was studied in [12]. Particularly, the scaled CL energy  $\varepsilon_c(b) = \varepsilon(w_{V34}(b), b) = \Delta E/(Z\langle 1/R \rangle)$  was graphed on a double-logarithmic scale, where  $\varepsilon$  is defined in (4) and  $w_{V34}$  is given by (A.7). It is presented in figure 6 by the solid curve; ‘lg  $x$ ’ stands for ‘ $\log_{10} x$ ’.

In figure 6 we have also presented plots of  $\varepsilon_c(b)$  for three different non-zero values of  $\lambda$ . A numerical value for  $w_{V34}$  was taken to increase precision.

From figure 6 we can see that the plasma screening decreases the value of CL in the ionization channel. Also, starting from about  $\lambda = 1.7$ , we observe the ‘cutoff’ value of  $b > 1$ , below which  $\varepsilon_c$  becomes negative, i.e., the electron energy at  $w_{V34}$  becomes positive. This means that there is no

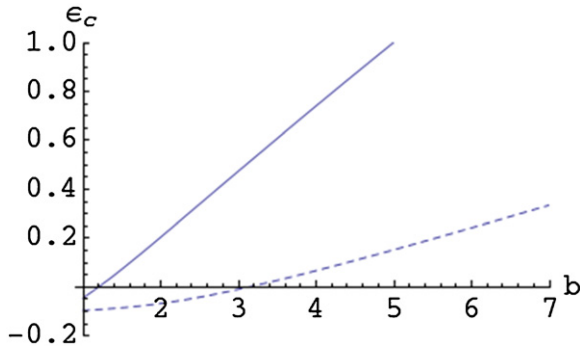


**Figure 7.** The plot of the continuum lowering (CL) energy versus  $b$  for  $\lambda = 2$  (solid curve) and  $\lambda = 3$  (dashed curve).

more CL in this ionization channel—instead, the continuum becomes higher than for the isolated hydrogen-like ion of the nuclear charge  $Z$ . This effect cannot be observed in the logarithmic graphs in figure 6 because the cutoff value of energy (zero) corresponds to  $\lg \varepsilon_c = -\infty$ . In figure 7, we have plotted the linear, non-logarithmic plots of  $\varepsilon_c(b)$  for selected values of  $\lambda$  at which this effect is observed.

In figure 7 we can see that at  $\lambda = 3$  there is no CL, for example, for  $b = 2$  and  $b = 3$ .

#### 4. Electric field effects on the continuum lowering in the ionization channel

Using the value of the scaled energy of the electron in the TCC system given in equation (5) of paper [20] with the substitution of the numeric or approximate solution for  $p$  from (10) into (5) and (7) and the further substitution of  $\ell$  from (7) into (5) (all equations are from [20]), we obtain the dependence of the scaled energy on the scaled coordinate  $w$  in the situation where the electric field is parallel to the internuclear axis:

$$\varepsilon = \frac{w^2 + p/2}{(w^2 + p)^{3/2}} + \frac{b((1-w)^2 + p/2)}{((1-w)^2 + p)^{3/2}} + fw, \quad (14)$$

where  $f = (R^2/Z)F$  is the scaled electric field and  $p$  is determined by the equation

$$f + \frac{b(1-w)}{((1-w)^2 + p)^{3/2}} = \frac{w}{(w^2 + p)^{3/2}}. \quad (15)$$

Then we numerically find the point on the  $w$ -axis corresponding to the V34 crossing for a given value of the scaled electric field  $f$ . The V34 crossing corresponds to the minimum of function  $r(w)$  for the given  $b$  and  $f$  (similar to (9)) in the range  $0 < w < w_1$ :

$$r = p^{-2} \left( \frac{1}{(w^2 + p)^{3/2}} + \frac{b}{((1-w)^2 + p)^{3/2}} \right)^{-1}, \quad (16)$$

where  $p$  is determined by (15) as well. We find numerically the value  $w$  of the minimum and substitute it into the formula for the scaled energy, obtaining the critical energy, which is the value of CL.

In figures 8–10, the logarithmic plots ( $\lg \varepsilon_c$  versus  $\lg b$ ) were made for selected values of  $f$ .

It is seen that CL increases as the electric field increases. This is expected because the electric field promotes ionization.

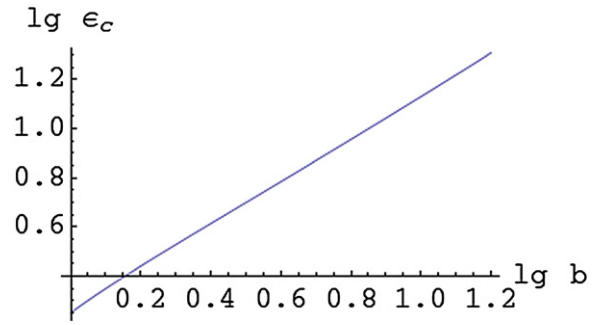


**Figure 8.** The plot of the continuum lowering (CL) energy versus  $b$  for  $f = 0.1$ .

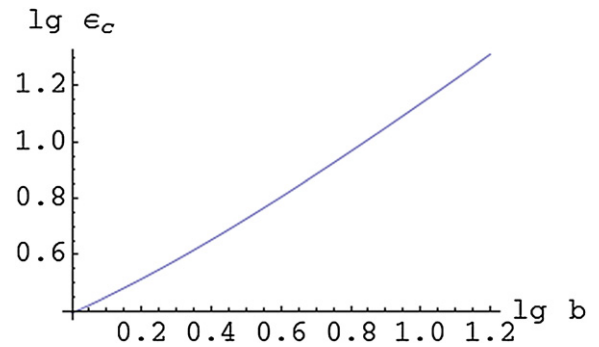


**Figure 9.** The plot of the continuum lowering (CL) energy versus  $b$  for  $f = 1$ .

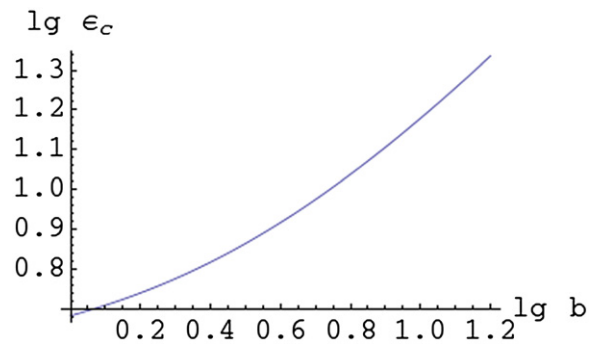


**Figure 10.** The plot of the continuum lowering (CL) energy versus  $b$  for  $f = 10$ .

#### 5. Magnetic field effects on the continuum lowering in the ionization channel

In the case of the magnetic field  $\mathbf{B}$  parallel to the internuclear axis, the default ( $\lambda = 0$ ) energy

$$E = \frac{L^2}{2\rho^2} - \frac{Z}{\sqrt{z^2 + \rho^2}} - \frac{Z'}{\sqrt{(R-z)^2 + \rho^2}} \quad (17)$$

will acquire an additional term

$$\Omega L + \frac{\Omega^2 \rho^2}{2} \quad (18)$$

where  $\Omega = B/(2c)$  is the Larmor frequency. We apply the same method as we used before to find the energy dependent on one spatial parameter. Substituting the scaled quantities as defined in (4) and defining  $\omega = \Omega L^3/Z^2$ , taking the derivatives by  $w$  and  $p$  and setting them equal to zero, solving for  $p$  and

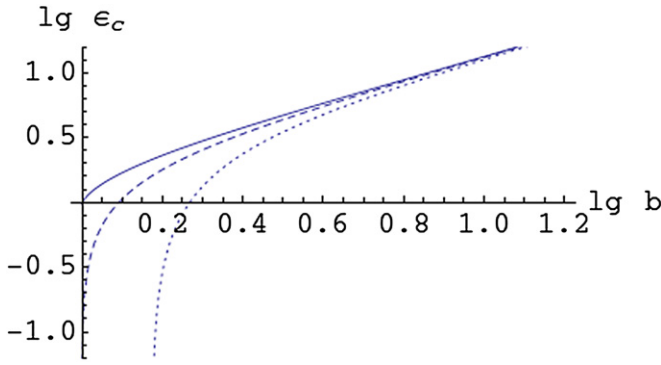


**Figure 11.** The plot of the continuum lowering (CL) energy versus  $b$  on a double-logarithmic scale for  $\omega = 0.5$  (solid curve),  $\omega = 1$  (dashed curve) and  $\omega = 2$  (dotted curve).

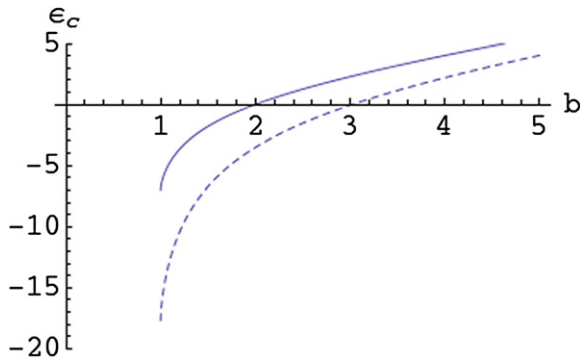


**Figure 12.** The plot of the continuum lowering (CL) energy versus  $b$  for  $\omega = 2.8$  (solid curve) and  $\omega = 4.3$  (dashed curve).

$\ell$ , substituting them back into the formula for energy, and further substituting the parameter  $\gamma$  as given in equation (A.3) in appendix A, we arrive at the following expressions of the scaled energy  $\varepsilon = -ER/Z$ ; and the scaled internuclear distance  $r$ :

$$\varepsilon = \frac{(\gamma^4 - 2\gamma + b^{2/3}(2\gamma^3 - 1))\sqrt{(\gamma^3 + 1)(b^{2/3}\gamma^2 - 1)}}{2\gamma(\gamma^3 - 1)^{3/2}} + \frac{\gamma^2(b^{2/3} - \gamma^4)}{(\gamma^3 + 1)^2(b^{2/3}\gamma^2 - 1)} \times \omega \left( \omega + \sqrt{\omega^2 + \frac{(\gamma^3 + 1)^{5/2}(b^{2/3}\gamma^2 - 1)^{3/2}}{\gamma^3(\gamma^3 - 1)^{3/2}}} \right), \quad (19)$$

$$r = \frac{(\gamma^3 + 1)^4(b^{2/3}\gamma^2 - 1)^2}{\gamma^4(b^{2/3} - \gamma^4)^2 \left( \omega^2 + \frac{(\gamma^3 + 1)^{5/2}(b^{2/3}\gamma^2 - 1)^{3/2}}{\gamma^3(\gamma^3 - 1)^{3/2}} \right)}. \quad (20)$$

To find the point of the V34 crossing, we take the derivative of  $r$  by  $\gamma$  and set it equal to zero. The numerical solution for this equation determines the value of  $\gamma$  corresponding to the minimum of  $r(\gamma)$  for given  $b$  and  $\omega$ , which corresponds to the crossing. Substituting it to the expression for the energy in (19), we obtain  $\varepsilon_c(b, \omega)$ —the dependence of CL on  $b$  for a given  $\omega$ .

In figures 11 and 12 we present several double-logarithmic plots, similar to those in the previous sections, for selected values of  $\omega$ .

From the graphs in figure 11 it is seen that the effect of the magnetic field on CL is similar to the effect of the plasma screening—it decreases CL. The ‘cutoff’ values of  $b$ , below which there is no CL for a given  $\omega$ , are also observed as  $\omega$  becomes large. From figure 12 it is seen, for example, that for  $\omega = 2.8$ , CL at  $b = 2$  vanishes, so the values of  $b$  corresponding to CL start at  $b > 2$ . At  $\omega = 4.3$ , the ‘cutoff’ value is  $b = 3$ .

## 6. Conclusions

We studied effects of the plasma screening, electric and magnetic fields on the value of continuum lowering (CL) in the ionization channel by employing the dicentre model of CL, to which the calculations of CL advanced from one-centre (ion sphere) models over recent years. By analysing physics of the corresponding one-electron Rydberg quasimolecules, we found that the screening and the magnetic field decrease the value of CL, inhibiting the ionization, while the electric field increases the value of CL, promoting the ionization. These results should be important for inertial fusion, x-ray lasers, powerful Z-pinchs, astrophysics and other applications of high-density plasmas.

We investigated also the effect of the screening on crossings of energy terms and on the stability of the nuclear motion of the corresponding Rydberg quasimolecules. We demonstrated that the screening stabilizes the nuclear motion in the case of  $Z = 1$  and destabilizes it in the case of  $Z > 1$ .

It should be noted that circular states of atomic and molecular systems, used in the present work, is an important subject in its own right. They have been extensively studied both theoretically and experimentally for several reasons (see, e.g., [20–36] and references therein): (a) they have long radiative lifetimes and highly anisotropic collision cross sections, thereby enabling experiments on inhibited spontaneous emission and cold Rydberg gases, (b) these classical states correspond to quantal coherent states, objects of fundamental importance, (c) a classical description of these states is the primary term in the quantal method based on the  $1/n$ -expansion, and (d) they can be used in developing atom chips. In the present paper we used circular states just to get the message across and to stimulate further studies of CL in the ionization channel.

## Appendix A. Crossings of the energy terms

Several properties of the classical energy terms have been studied. Using a small- $\lambda$  approximation by choosing (13) as the  $p(w)$  solution for the parametric energy terms (essentially, a zero- $\lambda$  approximation), we can substitute (13) into (9), which will give it the form below:

$$r = \frac{(1 - 2w)^{3/2} \sqrt{b^{2/3} - \left(\frac{w}{1-w}\right)^{2/3}}}{w^3 \left( b^{2/3} - \left(\frac{1-w}{w}\right)^{4/3} \right)^2}. \quad (A.1)$$

For a given  $b$ , the terms 3 and 4 are produced by varying  $w$  between 0 and  $w_1$ . The V34 crossing occurs at the value of  $w$  where  $r(w)$  has a minimum, as explained in [21, 22].

Therefore, setting the derivative  $dr/dw$  to zero, we obtain the equation whose solution for  $w$  in the range  $0 < w < w_1$  gives us the point on the parametric axis which produces the V34 crossing,

$$9w^{4/3}(1-w)^{4/3}(w^{4/3} + b^{4/3}(1-w)^{4/3}) = b^{2/3}(1-4w+22w^2-36w^3+18w^4). \quad (\text{A.2})$$

This equation has no dependence on  $\lambda$  and is therefore equivalent to the Coulomb-potential case ( $\lambda = 0$ ). It turns out that the form of the parametric dependence  $\varepsilon_1(r)$  in this case can be significantly simplified by introducing a new parameter

$$\gamma = \left(\frac{1}{w} - 1\right)^{1/3}. \quad (\text{A.3})$$

In this case,  $w = 0$  will correspond to  $\gamma = +\infty$  and  $w = 1$  will correspond to  $\gamma = 0$ , thus  $\gamma > 0$  in the allowed regions. The points  $w_1 = 1/(1+b^{1/2})$  and  $w_3 = b/(1+b)$  defining the allowed regions  $0 < w < w_1$ ,  $w_3 < w < 1$  (here we assume  $b > 1$ ) will correspond to  $\gamma_1 = b^{1/6}$  and  $\gamma_3 = 1/b^{1/3}$  (notice that  $0 < w < w_1$  corresponds to  $+\infty > \gamma > \gamma_1$  and  $w_3 < w < 1$  corresponds to  $\gamma_3 > \gamma > 0$ ). The energy terms  $\varepsilon_1(r)$  for the Coulomb-potential case will take the following parametric form:

$$\varepsilon_1(\gamma, b) = \frac{(b^{2/3} - \gamma^4)^2(\gamma(\gamma^3 - 2) + b^{2/3}(2\gamma^3 - 1))}{2(\gamma^3 - 1)^2(\gamma^6 - 1)}, \quad (\text{A.4})$$

$$r(\gamma, b) = \frac{\sqrt{b^{2/3}\gamma^2 - 1}(\gamma^6 - 1)^{3/2}}{\gamma(b^{2/3} - \gamma^4)^2}. \quad (\text{A.5})$$

The parametric plot of (A.4) and (A.5) with the parameter  $\gamma$  varied from 0 to  $1/b^{1/3}$  and from  $b^{1/6}$  to  $+\infty$  for  $b = 3$  will yield the same graph as in figure 3 in [22].

The crossing of the top two terms corresponds to the point where  $r(\gamma, b)$  has a minimum or  $\varepsilon_1(\gamma, b)$  has a maximum for a given  $b$ . Thus, taking the derivative of either function by  $\gamma$  and setting it equal to zero will yield a solution for the  $\gamma$  on the interval  $\gamma > 1$  corresponding to the crossing. The equation for  $\gamma$  obtained from differentiating  $r(\gamma)$  is a sixth-power polynomial and cannot be solved analytically; however, the equation for  $\gamma$  obtained from differentiating  $\varepsilon_1(\gamma)$  can be solved analytically for  $\gamma$ . Below is the critical value  $\gamma_0$  corresponding to the crossing

$$\gamma_0 = \sqrt{b^{1/3} + \frac{(b-1)^{1/3}}{b^{1/6}}((\sqrt{b}+1)^{1/3} + (\sqrt{b}-1)^{1/3})}. \quad (\text{A.6})$$

Therefore, an analytical solution exists for (A.2). Going back to the  $w$ -parametrization, we obtain the analytical solution of (A.2):

$$w_{V34} = \frac{1}{1 + \left(b^{1/3} + \frac{(b-1)^{1/3}}{b^{1/6}}((\sqrt{b}+1)^{1/3} + (\sqrt{b}-1)^{1/3})\right)^{3/2}}. \quad (\text{A.7})$$

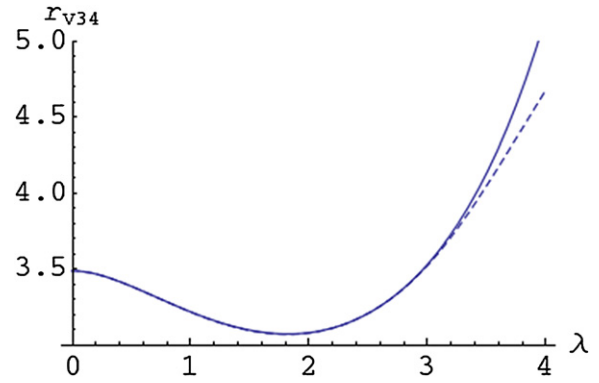


Figure A.1. Semi-analytical (solid curve) and numerical (dashed curve) plot of  $r_{V34}(\lambda)$  for  $b = 3$ .

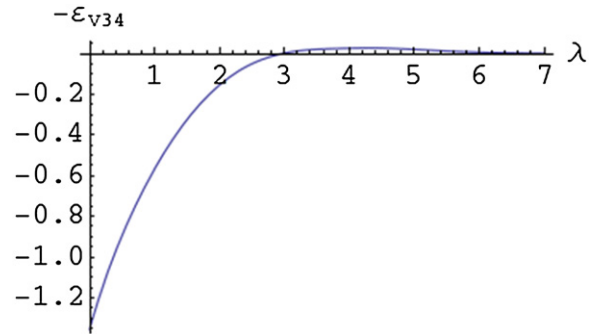


Figure A.2. Numerical plot of  $-\varepsilon_{V34}(\lambda)$  for  $b = 3$ .

Substituting it into (9) and using the numerical solution for  $p$  of (10), we obtain the semi-analytical dependence  $r_{V34}(\lambda)$  for a given  $b$ . Since it was obtained using a zero- $\lambda$  approximation for the point of the V34 crossing, we also graphed this dependence numerically point by point. Figure A.1 shows the semi-analytical (solid curve) and figure A.2 shows the numerical (dashed curve) plot for  $b = 3$ .

Figure A.1 shows that in relation to terms 3 and 4, this approximation works well even for moderate values of  $\lambda$ .

The energy of the V34 crossing can be obtained semi-analytically by substituting the numerical solution for  $p$  of (10) into (8), and by further substituting (A.7) into the resulting formula. It could be seen that as  $\lambda$  grows, the energy of the crossing grows and at a relatively large  $\lambda$  becomes positive. A numerical graph can also be made in a fashion similar to figure A.1. A visual comparison shows a good similarity between the two. Figure A.2 shows a numerical graph for  $b = 3$ .

As we see, the energy of the V34 crossing becomes positive after  $\lambda = 2.96$ , has a maximum, and later asymptotically approaches zero. For  $b = 4/3$ , the V34 crossing reaches zero energy at  $\lambda = 2.13$ .

The shape of terms 3 and 4 is also affected by the screening. Term 3, whose energy increases as  $r$  increases, becomes nearly horizontal at energy  $-0.5$  at a certain value of  $\lambda$ ; at further  $\lambda$ , its energy decreases with  $r$ . For  $b = 3$ , this value of  $\lambda$  is about 1.1; for  $b = 4/3$ , it is about 0.7. The plots of these are shown in figures A.3 and A.4.

For V12 crossing, the small- $\lambda$  approximation is not applicable since this crossing is not observed at  $\lambda = 0$ .

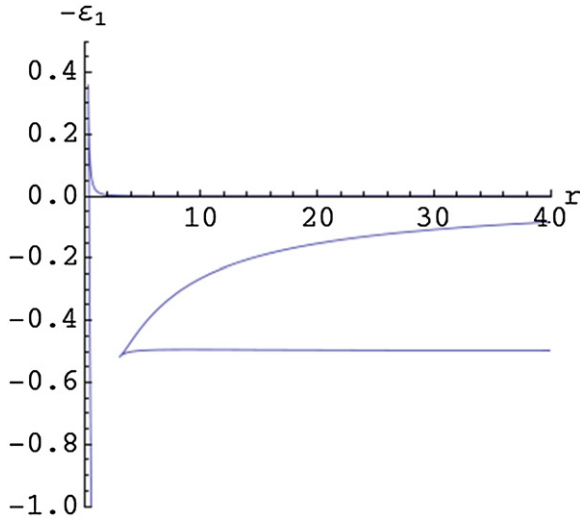


**Figure A.3.** Classical energy terms for  $b = 3$  at  $\lambda = 1.1$ ; term 3 is nearly constant at the energy  $-\varepsilon_1 = -0.5$ .

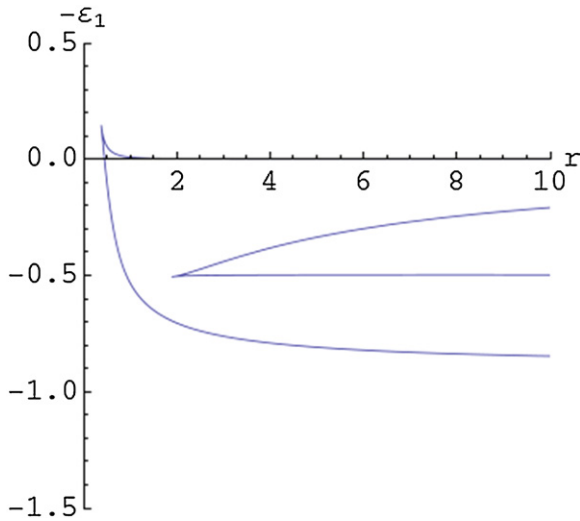


**Figure A.4.** The same as figure A.3, but for  $b = 4/3$  at  $\lambda = 0.7$ .

Therefore, only numerical methods were used. A situation of particular interest is the behaviour of term 1 at very small  $r$ , because as  $r \rightarrow 0$  it corresponds to the energy of the hydrogenic ion, plasma screening of which was studied in [23] (in our case, the nuclear charge of the hydrogenic ion is  $Z + Z'$ ). The point with the smallest  $r$  is the V12 crossing. A comparison was made of the dependence of the electronic energy on the screening parameter  $\lambda$  between the results from [23] and the limiting case  $r \rightarrow 0$  in our situation. Since in [23] the calculation was performed for a single Coulomb centre  $Z$ , we had to re-scale the quantities to make a valid comparison. The electronic energies are related as  $\varepsilon_1^{(\text{TCC})} = (1 + b)^2 \varepsilon_1^{(\text{OCC})}$ , where OCC stands for ‘one-Coulomb centre’. Since the scaling for the screening parameter in the OCC case did not include  $R$  (the internuclear distance), the scaling factor between the screening parameter includes  $r$ :  $\lambda^{(\text{TCC})} = r(1 + b)\lambda^{(\text{OCC})}$ . Taking this into account, we can plot the energy dependence on  $\lambda$  for the limiting case  $r \rightarrow 0$ .

Figure A.6 shows the dependence obtained in [23] for OCC:

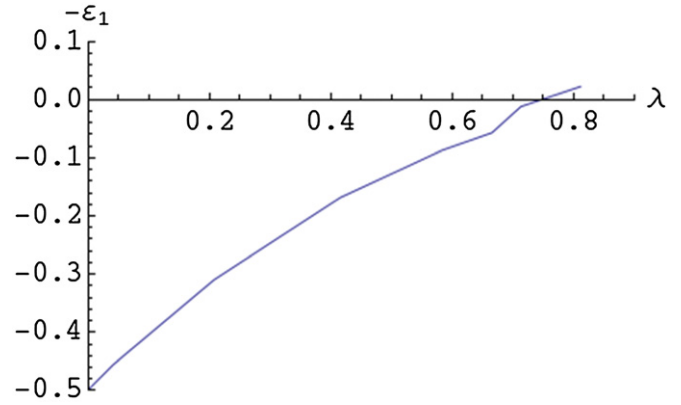


**Figure A.5.** Plot of the energy of the electron versus the scaled screening factor for  $b = 3$  in the limit  $r \rightarrow 0$ .

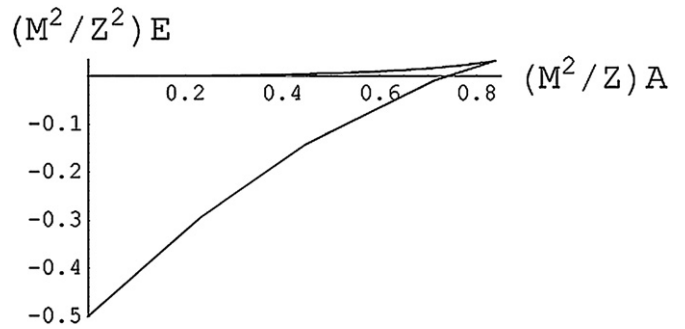


**Figure A.6.** Plot of the energy of the electron in a one-Coulomb centre (OCC) system versus the scaled screening factor.

### Appendix B. Effects of the plasma screening on the stability of the nuclear motion of Rydberg quasimolecules

Another aspect of this problem worth studying is the internuclear potential. Previously its properties were studied for the same system with  $\lambda = 0$  and a magnetic field parallel to the internuclear axis [24]. Particularly, the magnetic field created a deep minimum in the internuclear potential, which stabilized the nuclear motion and transformed a Rydberg quasi-molecule into a real molecule. Here we shall investigate the effect of the screening on the internuclear potential. Its form in atomic units is

$$U_{\text{int}} = \frac{ZZ'}{R} + E, \quad (\text{B.1})$$

where  $E$  is the electronic energy. Using the scaled quantities from (4), we have the scaled internuclear potential

$$u_{\text{int}} = \frac{bZ}{r} - \varepsilon_1, \quad (\text{B.2})$$

where  $U_{\text{int}} = (Z/L)^2 u_{\text{int}}$ . By plotting its dependence on  $r$ , we found out that in cases of  $Z > 1$  the screening tends to flatten the minimum, producing the effect opposite to the one of the magnetic field. Compare the plots of  $u_{\text{int}}(r)$  in the case of  $Z = 2$ ,  $b = 2$  for  $\lambda = 0$  and  $\lambda = 0.3$ .

The screening increases the potential of the point of intersection of the two branches; the upper branch, which has a very shallow minimum at  $\lambda = 0$ , loses it as  $\lambda$  increases.

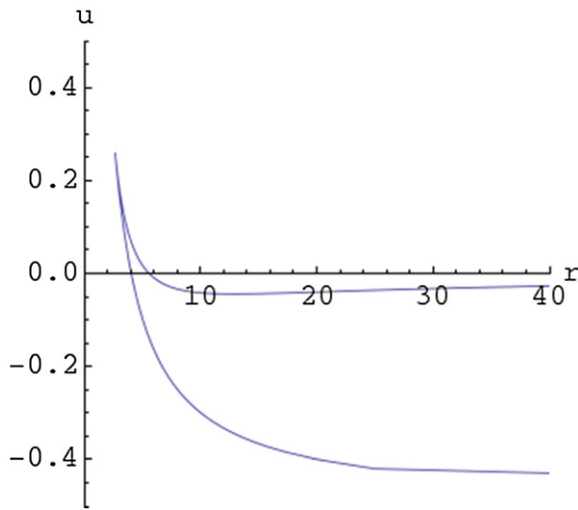


**Figure B.1.** The plot of the scaled internuclear potential versus the scaled internuclear distance for  $Z = 2, Z' = 4, \lambda = 0$ .

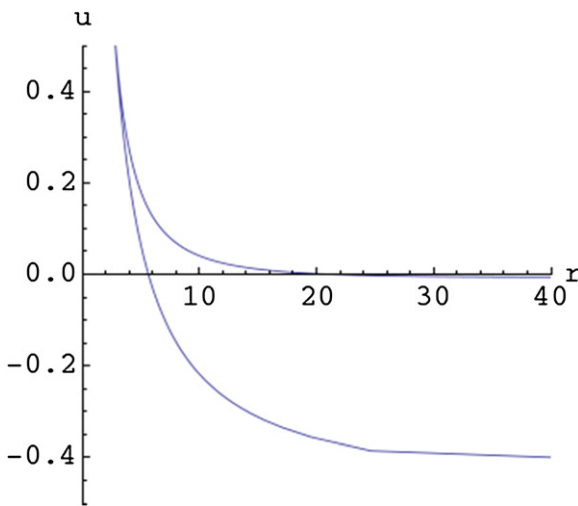


**Figure B.2.** The plot of the scaled internuclear potential versus the scaled internuclear distance for  $Z = 2, Z' = 4, \lambda = 0.3$ .

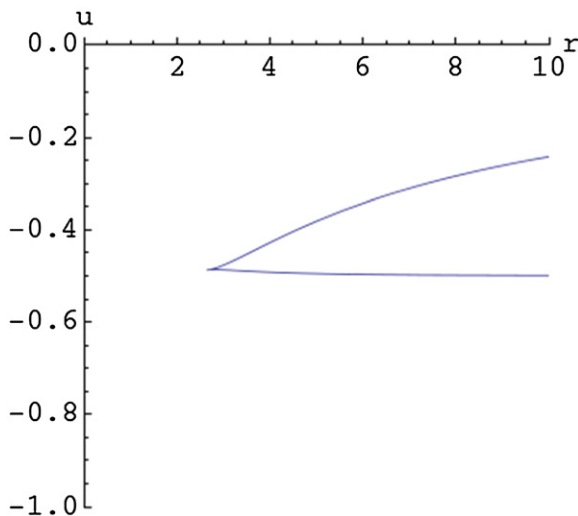


**Figure B.3.** The plot of the scaled internuclear potential versus the scaled internuclear distance for  $Z = 1, Z' = 2, \lambda = 0$ .

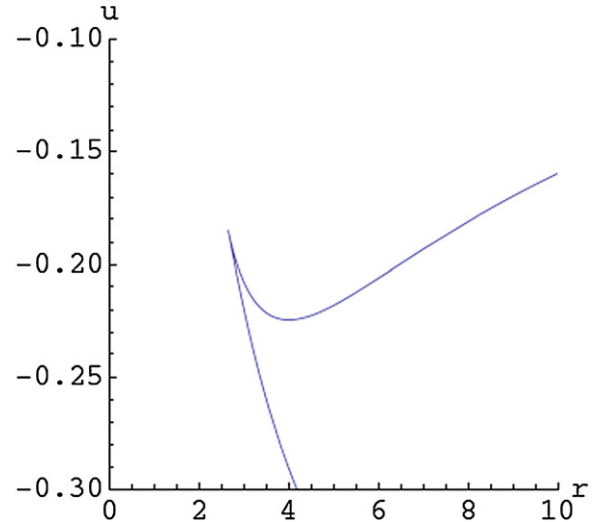


**Figure B.4.** The plot of the scaled internuclear potential versus the scaled internuclear distance for  $Z = 1, Z' = 2, \lambda = 0.3$ .

A completely different behaviour was observed for  $Z = 1$ . A small  $\lambda$  creates a deep minimum in the upper branch of the potential. For comparison, we present the plots of the potential in the case of  $Z = 1, b = 2$  for  $\lambda = 0$  and  $\lambda = 0.3$ .

Figures B.1–B.4 demonstrate that plasma screening stabilizes the nuclear motion for the case of  $Z = 1$ , but destabilizes it for  $Z > 1$ .

## References

- [1] Drake R P 2006 *High-Energy-Density-Physics: Fundamentals, Inertial Fusion, and Experimental Astrophysics* (Berlin: Springer) Section 3.2.2
- [2] Atzeni S and Meyer-ter-Vehn J 2004 *The Physics of Inertial Fusion: Beam Plasma Interaction, Hydrodynamics, Hot Dense Matter* (New York: Oxford University Press) Section 10.1.4.
- [3] Salzmann D 1998 *Atomic Physics in Hot Plasmas* (Oxford: Oxford University Press) chapters 2, 3
- [4] Murillo M S and Weisheit J C 1998 *Phys. Rep.* **302** 1
- [5] Griem H R 1997 *Principles of Plasma Spectroscopy* (Cambridge: Cambridge University Press) Sections 5.5, 7.3
- [6] Stein J, Goldberg I B, Shalitin D and Salzmann D 1989 *Phys. Rev. A* **39** 2078
- [7] Salzmann D, Stein J, Goldberg I B and Pratt R H 1991 *Phys. Rev. A* **44** 1270
- [8] Stein J and Salzmann D 1992 *Phys. Rev. A* **45** 3943
- [9] Malnoul P, D'Etat B and Nguen H 1989 *Phys. Rev. A* **40** 1983
- [10] Furutani Y, Ohashi K, Shimizu M and Fukuyama A 1993 *J. Phys. Soc. Japan* **62** 3413
- [11] Sauvan P, Leboucher-Dalimier E, Angelo P, Derfoul H, Ceccotti T, Poquerusse A, Calisti A and Talin B 2000 *J. Quant. Spectrosc. Radiat. Transfer* **65** 511
- [12] Oks E 2001 *Phys. Rev. E* **63** 057401
- [13] Lee E, Farrelly D and Uzer T 1997 *Opt. Express* **1** 221
- [14] Germann T C, Herschbach D R, Dunn M and Watson D K 1995 *Phys. Rev. Lett.* **74** 658
- [15] Cheng C H, Lee C Y and Gallagher T F 1994 *Phys. Rev. Lett.* **73** 3078
- [16] Chen L, Cheret M, Roussel F and Spiess G 1993 *J. Phys. B: At Mol. Opt. Phys.* **26** L437
- [17] Hora H 1991 *Plasmas at High Temperature and Density* (Berlin: Springer) Section 12.4

- [18] Rose S J (ed) 1995 *Laser Interaction with Matter: Proc. 23rd European Conf. (Oxford 1994)* (Institute Of Physics Conference Series No. 140) (Bristol: Institute of Physics) pp 173 215, 221
- [19] Liberman M A, De Groot J S, Toor A and Spielman R B 1999 *Physics of High-Density Z-Pinch Plasmas* (New York: Springer)
- [20] Kryukov N and Oks E 2012 *Can. J. Phys.* **90** 647
- [21] Oks E 2000 *Phys. Rev. Lett.* **85** 2084
- [22] Oks E 2000 *J. Phys. B: At. Mol. Opt. Phys.* **33** 3319
- [23] Flannery M R and Oks E 2008 *Eur. Phys. J. D* **47** 27
- [24] Flannery M R and Oks E 2006 *Phys. Rev. A* **73** 013405
- [25] Nogues G, Lupascu A, Emmert A, Brune M, Raimond J-M and Haroche S 2011 *Atom Chips* ed J. Reichel and V Vuletic (Weinheim: Wiley) chapter 10, Section 10.3.3
- [26] Tan J N, Brewer S M and Guise N D 2011 *Phys. Scr.* **T144** 014009
- [27] Kryukov N and Oks E 2012 *Int. Rev. At. Mol. Phys.* **3** 17
- [28] Dehesa J S, Lopez-Rosa S, Martinez-Finkelshtein A and Janez R J 2010 *Int. J. Quantum Chem.* **110** 1529
- [29] Nandi T 2009 *J. Phys. B: At. Mol. Opt. Phys.* **42** 125201
- [30] Jentschura U D, Mohr P J, Tan J N and Wundt B J 2008 *Phys. Rev. Lett.* **100** 160404
- [31] Shytov A V, Katsnelson M I and Levitov L S 2007 *Phys. Rev. Lett.* **99** 246802
- [32] Devoret M, Girvin S and Schoelkopf R 2007 *Ann. Phys.* **16** 767
- [33] Oks E 2004 *Eur. Phys. J. D* **28** 171
- [34] Holmlid L 2002 *J. Phys.: Condens. Matter.* **14** 13469
- [35] Dutta S K, Feldbaum D, Walz-Flannigan A, Guest J R and Raithel G 2001 *Phys. Rev. Lett.* **86** 3993
- [36] Carlsen H and Goscinski O 1999 *Phys. Rev. A* **59** 1063